Magnetostrictive bimagnetic trilayer ribbons for temperature sensing

P. Mendoza Zélis[a)]
Departamento de Física-FCE, Universidad Nacional de La Plata, C.C. 67, 1900 La Plata, Argentina and Instituto de Ciencia de Materiales, CSIC, Canto Blanco, 28049 Madrid, Spain

F. Sánchez
Departamento de Física-FCE, Universidad Nacional de La Plata, C.C. 67, 1900 La Plata, Argentina

M. Vázquez
Instituto de Ciencia de Materiales, CSIC, Canto Blanco, 28049 Madrid, Spain

(Received 22 March 2006; accepted 2 November 2006)

A magnetic biphase trilayer ribbon, consisting of a melt-spun FeSiB inner amorphous ribbon with positive magnetostriction coated by two electroplated nickel layers with negative magnetostriction, is here proposed as an element to be incorporated in temperature sensor devices. The inductance of a small coil wounded around the trilayer is characterized as the sensitive parameter. The dependence of coil's inductance on the thickness of electroplated Ni has been evaluated in the range of measuring temperatures of 0–70 °C, and optimum electroplating parameters were determined. Magnetic characteristics are determined through the study of hysteresis loops, which denote the presence of the two magnetic phases. The experimental results are interpreted considering a simple magnetoelastic model taking into account the mechanical stresses arising from the different thermal expansion coefficients of each magnetic phase.
[DOI: 10.1063/1.2422905]

INTRODUCTION

Amorphous magnetically soft alloys are of technological interest in a number of applications, as cores in small transformers and motors, and particularly as sensing elements in various devices profiting of their excellent magnetic response at high frequency and their sensitivity to applied stresses.[1–3] Due to their amorphous nature, magnetocrystalline anisotropy averages to zero and magnetoelastic anisotropy, $e_{me} \approx \lambda\sigma$, proportional to magnetostriction λ and to mechanical stress σ determines their general magnetic properties. Consequently, amorphous alloys with large magnetostriction, as the Fe–Si–B ones, are suitable to be used as elements in magnetoelastic sensor devices. They can be used to sense stresses[1,4,5] and indirectly to evaluate properties associated with the stress as, for example, flux of gases and liquids, acceleration, curvature, etc.[5–7] For a comprehensive survey of magnetoelastic sensors see Ref. 8.

Bimetal sensing elements are currently used in a number of applications.[6,9] A particular useful case is that of trilayer elements where a central layer is symmetrically covered by two layers of a different material.[10] These sensing elements typically consist of a magnetostrictive layer (MSL), for instance, a melt-spun amorphous ribbon, and two counterlayers (CLs) generally chosen to be nonmagnetic, which transfer stress to the magnetic component. Typically, the layers are fixed to each other by a suitable gluing layer (GL), so that the magnetic response of the MSL is modified as a consequence of the magnetoelastic effect. These systems have been proposed in thermal sensors based on the magnetoelastic coupling arising from the different thermal expansion coefficients of MSL and CLs.[7] Nevertheless, although a nice response can be attained, a technical problem arises from the gluing itself, because the GL absorbs a considerable fraction of the stress, thus limiting the sensitivity of the element. Besides, gluing may potentially lead to dissimilarities among otherwise alike devices, or to nonrepetitive performances, due to slight differences among the GLs and their degradation with aging.[7]

In the present work, a type of bimagnetic magnetostrictive trilayer sensing elements is proposed. A first innovation has been the use of the electrodeposition technique to grow the counterlayers onto the central magnetic layer, that is without an intermediate GL, following a methodology employed to produce multilayer magnetic microwires.[11] Simultaneously, this innovation is also being used to show the magnetostatic coupling between magnetic layers.[12] The proposed fabrication method produces more robust devices, with repetitive and enhanced sensing performance. A second innovation is that the counterlayers have been here selected to exhibit also significant magnetostriction whose sign is opposite to that of the MSL. This leads to additional cooperative changes in the magnetic state (i.e., permeability) of the trilayer when submitted to stresses of thermal origin. It also allows us to select materials with not so different thermal expansion coefficients and therefore to keep the thermal stress at sufficiently low values as to produce an approximately linear dependence of permeability versus stress. In this way, the exclusion of relatively high stress values not only favors the durability of sensing elements but also gives rise to an approximately linear response to temperature changes.

The temperature dependence of the inductance of a pickup coil wounded around the sensing element, propor-

[a)]Electronic mail: pmendoza@fisica.unlp.edu.ar

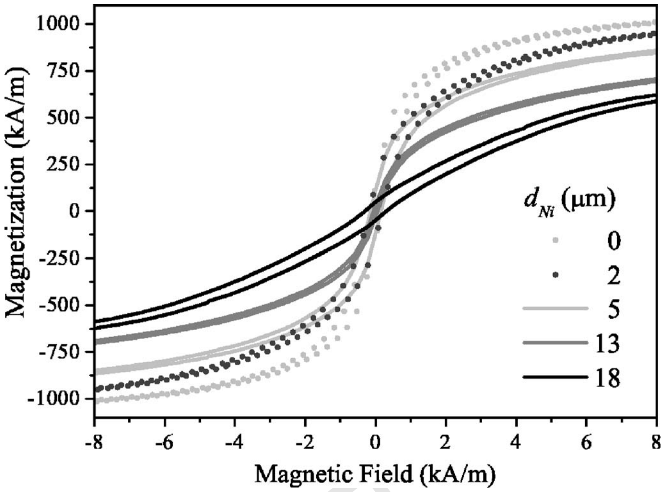

FIG. 1. Low-field region of the hysteresis loops for trilayers with different Ni thicknesses.

tional to its permeability, has been determined in the temperature range between 0 and 70 °C. For this particular experiment we have electroplated a negative magnetostriction nickel layer on each side of a positive magnetostriction melt-spun $Fe_{75}Si_{15}B_{10}$ amorphous ribbon. Experiments have been performed for different times and density electrodeposition currents to control the counterlayer's thickness and its properties.

We have developed a simple magnetic model that introduces a semiquantitative interpretation of the thermal and magnetoelastic features of the composite material, particularly the trilayer susceptibility and coil inductance dependences on temperature and CL thickness. This model gives a fair account for the experimental finding of the existence of an optimum CL thickness value.

EXPERIMENTAL METHODS AND RESULTS

An amorphous alloy ribbon with $Fe_{75}Si_{15}B_{10}$ nominal composition, positive magnetostriction $\lambda_{am} \approx +32 \times 10^{-6}$, thermal expansion coefficient $\alpha_{am} = 11.8 \times 10^{-6}$ K^{-1}, and Young's modulus $E_{am} \approx 160$ GPa, has been selected for the inner magnetic layer, MSL. The mother alloy was prepared by arc melting the constituent elements in argon atmosphere. The amorphous ribbon was prepared in our laboratory by melt spinning in argon atmosphere onto a single copper wheel, rotating with a surface speed of 38 m/s. Final thickness and width of the obtained samples have been $d_{am} = 22$ μm and $h = 0.7$ mm, respectively.

Two Ni layers (CLs) with nominal characteristics of $\lambda_{Ni} \approx -40 \times 10^{-6}$, $\alpha_{Ni} = 13.4 \times 10^{-6}$ K^{-1}, and $E_{Ni} \approx 200$ GPa, were electrochemically grown onto each surface of the amorphous layer with the help of a especially designed electrochemical cell. The electrolyte composition was H_3BO_3 (45 g/l), $NiCl_2 \cdot 6H_2O$ (45 g/l), and $NiSO_4 \cdot 6H_2O$ (300 g/l), and its temperature during electrodeposition was kept at 315 K. Thickness of the deposited cover was controlled through the deposition time (ranging up to 2 h) and dc current density (typically 0.24 mA/cm^2) and measured with a digital micrometer. The length of the trilayer was 28 mm.

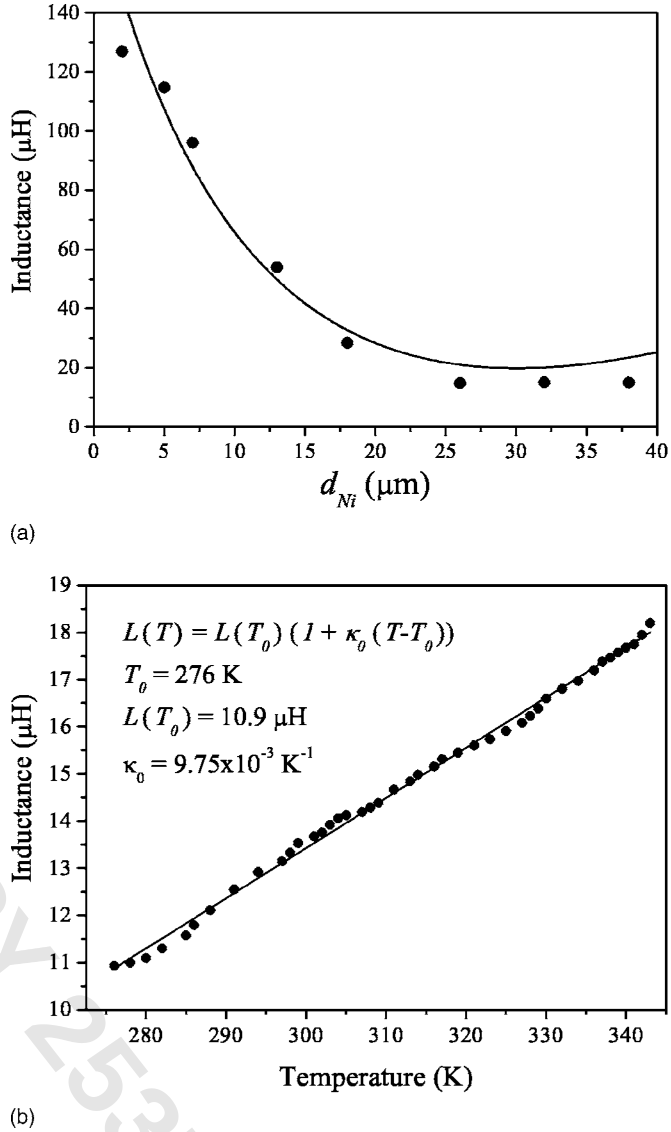

FIG. 2. Dependence of the pickup coil inductance on Ni thickness (a) and on temperature (b). Experimental measurements (dots) and model prediction (line) are shown.

The magnetic characterization of the trilayer elements has been carried on with a vibrating sample magnetometer (VSM) at room temperature under a maximum applied field of 1 T. Figure 1 shows the low-field region of the hysteresis loops of different trilayers for a range of Ni thickness. The reduction of low-field susceptibility and remanent magnetization with Ni thickness must be ascribed to the harder magnetic character of this element, as it will be later analyzed.

A pickup coil, 450 turns and 3 cm long, was wounded around a glass capillary tube, 1 mm outer diameter, where the trilayer was inserted. The inductance L of such a coil was measured with an HP4284 *LCR* meter at a frequency of 10 kHz. Its experimental dependence on the thickness of the electroplated Ni layers, measured at 18 °C, is shown in Fig. 2(a) (dots). As observed, the inductance decreases monotonically with the Ni layer thickness.

To study the changes of the magnetic response of the sensing element with temperature, we measured the temperature dependence of the coil's inductance. The set composed of pickup coil and trilayer was placed inside a de-ionized water bath where the temperature was controlled between 0 and 70 °C. As an example, Fig. 2(b) shows the evolution of the inductance with temperature for a sample with 13 μm total Ni thickness.

MAGNETOELASTIC MODELING AND ANALYSIS OF EXPERIMENTAL RESULTS

In this section we introduce a simple model in order to interpret the previous experimental results, particularly those related to the coil self-inductance, when the trilayer is used as its core. This model is based on the magnetoelastic coupling between the strongly bounded amorphous and Ni layers, and its effect on the trilayer permeability and therefore on the coil inductance.

Since the chosen temperature interval for the study is relatively small, $\Delta T \ll T_C$ (where T_C is the Curie temperature of any of the system components), and temperature itself is well below T_C, the model does not take into account the small permeability changes arising from variations of saturation magnetization with temperature.

When the temperature departs from electrodeposition temperature T_e, internal stresses arise owing to the mechanical link among the MSL (amorphous) and CL (nickel) layers and to their different thermal expansion coefficients. The combined effect is to induce opposite stresses on the MSL and CLs which are proportional to the thermal strains. Due to the small thicknesses of the layers of our samples, we will use, for the sake of simplicity, a model that assumes that the stresses that arise in each one of them are distributed homogeneously generating a homogenous deformation of each layer. Under these conditions, a simple analysis immediately leads to the following expressions for the stress on each layer:

$$\sigma_{\rm am} = (\alpha_{\rm tri} - \alpha_{\rm am}) E_{\rm am} \Delta T, \tag{1a}$$

$$\sigma_{\rm Ni} = (\alpha_{\rm tri} - \alpha_{\rm Ni}) E_{\rm Ni} \Delta T, \tag{1b}$$

where $\alpha_{\rm tri}$ is the trilayer system effective thermal expansion coefficient and $\Delta T = T - T_e$. Applying the equilibrium condition among the forces acting on the layers is possible to obtain an expression for $\alpha_{\rm tri}$,

$$\alpha_{\rm tri} = \frac{\alpha_{\rm am} E_{\rm am} d_{\rm am} + \alpha_{\rm Ni} E_{\rm Ni} d_{\rm Ni}}{E_{\rm am} d_{\rm am} + E_{\rm Ni} d_{\rm Ni}}, \tag{2}$$

where $d_{\rm am}$ is the amorphous layer thickness and $d_{\rm Ni}$ is the total Ni layer thickness (the thickness of each Ni layer is thus $d_{\rm Ni}2$). Using Eq. (2) the stresses can be rewritten as

$$\sigma_{\rm am} = (\alpha_{\rm Ni} - \alpha_{\rm am}) \frac{E_{\rm am} E_{\rm Ni} d_{\rm Ni}}{E_{\rm am} d_{\rm am} + E_{\rm Ni} d_{\rm Ni}} \Delta T, \tag{3a}$$

$$\sigma_{\rm Ni} = (\alpha_{\rm am} - \alpha_{\rm Ni}) \frac{E_{\rm am} E_{\rm Ni} d_{\rm am}}{E_{\rm am} d_{\rm am} + E_{\rm Ni} d_{\rm Ni}} \Delta T. \tag{3b}$$

As a consequence of the appearance of such stresses, the corresponding magnetoelastic contribution to the energy density, $e_{\rm me} \sim \lambda \sigma$, will modify the composite magnetic response, in particular, its effective permeability μ, which will be a function of T and $d_{\rm Ni}$. Therefore, the self-inductance L of a pickup coil having the trilayer as its core will also depend on these two quantities, as it is indeed experimentally observed [see Figs. 2(a) and 2(b)].

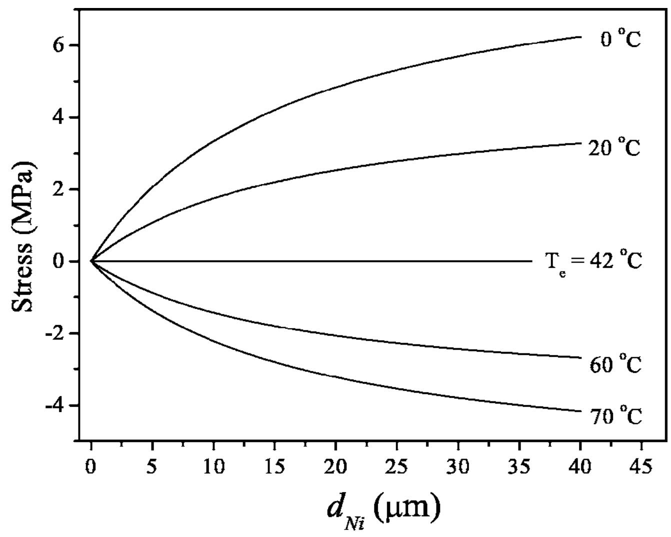

FIG. 3. Stress developed in the amorphous ribbon as a function of Ni thickness and temperature, calculated through Eq. (3a).

In Eqs. (3), stresses depend on the elastic modulus of each component, on the temperature, and on the thickness of plated Ni. Considering the particular parameters of the layers, an estimation of the stress arising in the amorphous ribbon as a function of the Ni thickness and of the temperature is presented in Fig. 3.

For the range of small induced stresses (note that they remain below 10 MPa), relative permeability $\mu^r = \mu^r(\lambda\sigma) = \mu(\lambda\sigma)/\mu_0$ of each layer can be assumed to exhibit a linear evolution with stress as

$$\mu^r_{\rm am} = \mu^{r\prime}_{\rm am} + \eta_{\rm am} \lambda_{\rm am} \sigma_{\rm am}, \tag{4a}$$

$$\mu^r_{\rm Ni} = \mu^{r\prime}_{\rm Ni} + \eta_{\rm Ni} \lambda_{\rm Ni} \sigma_{\rm Ni}, \tag{4b}$$

where η is a positive proportionality constant, and $\mu^{r\prime} = \mu^r(\sigma=0)$ is the relative permeability of the material at zero applied stress (in our case, for $T = T_e$). In fact, from available experimental data on Ni magnetization and magnetostriction under applied stress,[13] the approximate linearity between μ^r and σ as well as the constancy of λ (within about 1%) can be confirmed for the stresses appearing under our working conditions. It is even possible to estimate the stress derivative of relative permeability and from it, knowing λ, $\eta = (1/\lambda) \times (\partial \mu^r / \partial \sigma) \approx 1\ {\rm Pa}^{-1}$.

Introducing Eqs. (3) into Eqs. (4) we can express the relative permeability for each layer as

$$\mu^r_{\rm am} = \mu^{r\prime}_{\rm am} + \eta_{\rm am} \lambda_{\rm am} (\alpha_{\rm Ni} - \alpha_{\rm am}) \frac{E_{\rm am} E_{\rm Ni} d_{\rm Ni}}{E_{\rm am} d_{\rm am} + E_{\rm Ni} d_{\rm Ni}} \Delta T, \tag{5a}$$

$$\mu^r_{\rm Ni} = \mu^{r\prime}_{\rm Ni} + \eta_{\rm Ni} \lambda_{\rm Ni} (\alpha_{\rm am} - \alpha_{\rm Ni}) \frac{E_{\rm am} E_{\rm Ni} d_{\rm am}}{E_{\rm am} d_{\rm am} + E_{\rm Ni} d_{\rm Ni}} \Delta T. \tag{5b}$$

In order to correlate the trilayer permeability with the coil's inductance, let us consider a solenoid of N turns and length l, along which a current i circulates creating at its central region a longitudinal magnetic field $H=iN/l$. The trilayer ribbon is placed inside that region of the solenoid, which picks up a total flux that can be expressed as the addition of the fluxes across air, amorphous, and nickel, $\Phi=\Phi_0+\Phi_{\mathrm{am}}+\Phi_{\mathrm{Ni}}$. Then, then coil's inductance L can be expressed as

$$L(\mu_o A_o+\mu_{\mathrm{am}}A_{\mathrm{am}}+\mu_{\mathrm{Ni}}A_{\mathrm{Ni}})N^2/l \tag{6}$$

and corresponds to three inductances in series L_0, L_{am}, and L_{Ni}, being A_0, $A_{\mathrm{am}}=hd_{\mathrm{am}}$, and $A_{\mathrm{Ni}}=hd_{\mathrm{Ni}}$ the coil fractional cross sections filled with air, amorphous, and Ni, respectively.

AQ: #3 Introducing Eqs. (5) into Eq. (6), we obtain

$$\frac{L}{\mu_o N^2/l}=A_o+\mu_{\mathrm{am}}^{r\prime}d_{\mathrm{am}}h+\mu_{\mathrm{Ni}}^{\prime}d_{\mathrm{Ni}}h+h(\alpha_{\mathrm{Ni}}-\alpha_{\mathrm{am}})\times\frac{E_{\mathrm{am}}d_{\mathrm{am}}E_{\mathrm{Ni}}d_{\mathrm{Ni}}}{E_{\mathrm{am}}d_{\mathrm{am}}+E_{\mathrm{Ni}}d_{\mathrm{Ni}}}(\eta_{\mathrm{am}}\lambda_{\mathrm{am}}-\eta_{\mathrm{Ni}}\lambda_{\mathrm{Ni}})(T-T_e), \tag{7}$$

where h is the trilayer width.

Equation (7) allows us to evaluate the coil self-inductance as a function of d_{Ni} and T and to compare it with the experimental data. The coil's inductance can be rewritten in a general form as

$$L(T)=L_{T_e}[1+\kappa_e(T-T_e)], \tag{8}$$

being L_{T_e} the inductance at $T=T_e$,

$$L_{T_e}=(\mu_o A_o+\mu_{\mathrm{am}}^{\prime}A_{\mathrm{am}}+\mu_{\mathrm{Ni}}^{\prime}A_{\mathrm{Ni}})N^2/l, \tag{9}$$

and κ_e the sensitivity of the coil's inductance to temperature,

$$\kappa_e=\frac{(\alpha_{\mathrm{Ni}}-\alpha_{\mathrm{am}})(\eta_{\mathrm{am}}\lambda_{\mathrm{am}}-\eta_{\mathrm{Ni}}\lambda_{\mathrm{Ni}})}{A_o+\mu_{\mathrm{am}}^{r\prime}A_{\mathrm{am}}+\mu_{\mathrm{Ni}}^{r\prime}A_{\mathrm{Ni}}}\left(\frac{E_{\mathrm{am}}A_{\mathrm{am}}E_{\mathrm{Ni}}A_{\mathrm{Ni}}}{E_{\mathrm{am}}d_{\mathrm{am}}+E_{\mathrm{Ni}}d_{\mathrm{Ni}}}\right). \tag{10}$$

Equation (8) expresses that for modest temperature changes, when induced stresses are small enough, a linear temperature response of the inductance is expected. This has been clearly verified in the experiments. The experimental data shown in Fig. 2(b) have been fitted to a linear function with a temperature sensitivity of the coil of $\kappa_0=9.75\times10^{-3}\ \mathrm{K}^{-1}$ and $T_0=276$ K (in the fitting, the reference temperature is 276 K instead of T_e). The percent sensitivity, defined as the fractional change of inductance per temperature unit, $(\Delta L/L\Delta T)(\%)=100[(L-L_0)/L_0][1/(T-T_0)]=100\kappa_0$, is of about 1% K^{-1} and remains nearly constant in the whole investigated temperature interval. This value enables the sensing of temperature by using standard, nonexpensive meters.[10]

Let us now analyze the influence of Ni thickness. Figure 2(a) illustrates the evolution predicted by Eq. (7) of inductance with Ni layer thickness and its comparison with the experimental result. As observed and in spite of the simplicity of the model, it is remarkable that it reproduces the main characteristics of the inductance experimental dependences on T and d_{Ni}. As a function of d_{Ni}, the inductance first decreases from its initial value (coil filled with air and the amorphous ribbon) due to the increase of the magnetoelastic effect (fourth term of the equation) and, beyond 30 μm, it increases because this effect begins to saturate while the one originated by the replacement of Ni for air (third term) becomes dominant.

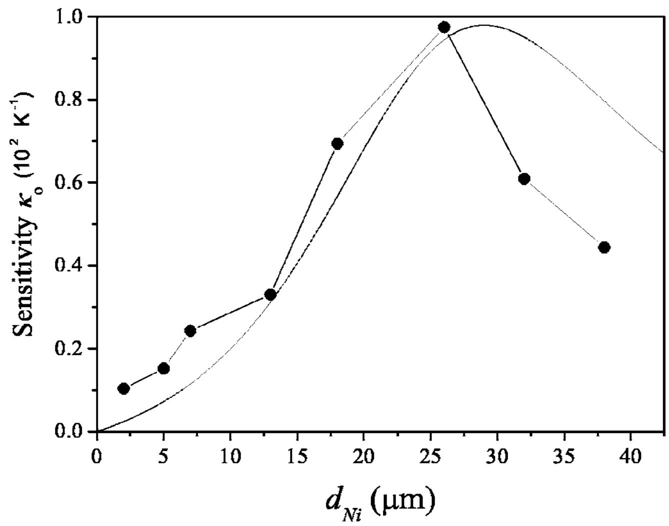

FIG. 4. Sensitivity κ_0 as a function of Ni thickness. Experimental measurements (dots) and model prediction (line) are shown.

It is also possible to carry out a deeper analysis of the sensor sensitivity. Measurements of the sensitivity for different Ni thicknesses were carried out (Fig. 4). They show that optimum sensitivity $\kappa_{\max}$ is achieved for a finite Ni layer thickness, $d_{\mathrm{Ni}}^{\max}$. In this figure we also show the curve κ versus d_{Ni} obtained from Eq. (10). This curve agrees semiquantitatively with the experimental results, displaying a $\kappa_{\max}$ value for a thickness $d_{\mathrm{Ni}}^{\max}$, which is obtained from the condition $\partial\kappa_e/\partial d_{\mathrm{Ni}}=0$,

$$d_{\mathrm{Ni}}^{\max}=[E_{\mathrm{am}}d_{\mathrm{am}}(A_o\mu_o+hd_{\mathrm{am}}\mu_{\mathrm{am}})/(E_{\mathrm{Ni}}h\mu_{\mathrm{Ni}})]^{1/2}. \tag{11}$$

Furthermore, the experimental and the model predicted $d_{\mathrm{Ni}}^{\max}$ values are in reasonable agreement, both having values of around 25 μm.

The experimental sensitivity peaks are rather sharp, indicating that the thickness of the electrodeposited layers must be carefully estimated and controlled. Sensor sensitivity measurements for different electrodeposition current densities, below 1 $\mathrm{mA/cm^{-2}}$, have been carried out. We found that the $d_{\mathrm{Ni}}^{\max}$ value also depends on the current density, although it remained within 5–30 μm for this range of current densities. It is well known that mechanical characteristics of materials (hardness, Young's modulus, percent of elastic recovery, etc.) are intimately related to microstructural properties (grain size, preferred grain orientation, grain boundaries, global materials density, dislocation density, etc), properties which are expected to depend on deposition speed, i.e., on current density. Thus, current density may provide a means of controlling sensing properties via the microstructure.[13] On the other hand, we have found that the experimental $\kappa_{\max}$ values were nearly nondependent on current density; therefore high densities may be preferred for sensing element industrial production in order to reduce the production time.

In order to gain direct information on the role of the Ni layer thickness on the permeability of the trilayer system and

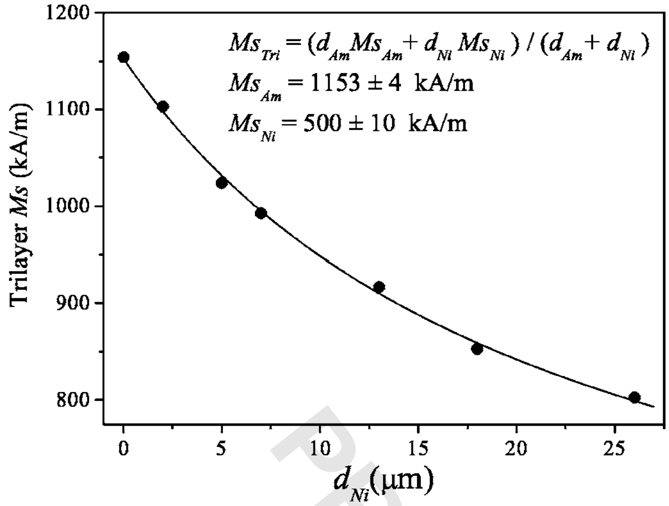

FIG. 5. Dependence of trilayer saturation magnetization on Ni layer thickness.

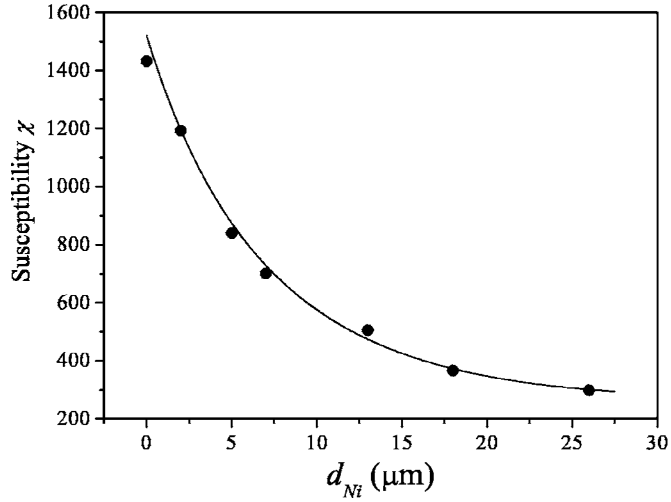

FIG. 6. Evolution of experimental initial susceptibility (dots) and model prediction (line), with thickness of Ni layer.

other basic properties, the analysis of magnetic data from hysteresis loops is presented. Saturation magnetization, $M_{s_{\mathrm{tri}}}$, was estimated by examining the high-field region of the hysteresis loops (see Fig. 5). $M_{s_{\mathrm{tri}}}$ values decrease monotonically with Ni layer thickness as expected from the particular values of the saturation magnetization ($M_{s_{\mathrm{am}}}, M_{s_{\mathrm{Ni}}}$) of the amorphous alloy and Ni, since $M_{s_{\mathrm{am}}} > M_{s_{\mathrm{Ni}}}$. An analysis of the evolution of $M_{s_{\mathrm{tri}}}$ with Ni thickness can be done taking into account the fractional contributions from the amorphous and Ni layers as

$$M_{s_{\mathrm{tri}}} = (M_{s_{\mathrm{am}}} d_{\mathrm{am}} + M_{s_{\mathrm{Ni}}} d_{\mathrm{Ni}})/(d_{\mathrm{am}} + d_{\mathrm{Ni}}). \tag{12}$$

A fitting of Eq. (12) to experimental data is shown in Fig. 5, where the optimum values obtained for the fitting parameters are $M_{s_{\mathrm{am}}} = 1153 \pm 4$ and $M_{s_{\mathrm{Ni}}} = 500 \pm 10$ kA/m, in fair agreement with the reported values of saturation magnetizations of $Fe_{75}Si_{15}B_{10}$ amorphous alloy[14] and of fcc-Ni.[15] This suggests that the magnetoelastic effects on the saturation magnetization values are negligible and also confirms the reliability of the thickness measurements.

Additional information can be obtained by analyzing in more detail the low-field region of the loops in Fig. 1. Low-field susceptibility decreases noticeably with Ni layer thickness, while a more moderate reduction of remanence is observed (which at least in part arises from the reduction of saturation magnetization shown in Fig. 5). Figure 6 shows the evolution of the experimental low-field susceptibility with d_{Ni}. Susceptibility contains again two contributions: from the amorphous and from the Ni layers,

$$\chi_{\mathrm{tot}} \approx \mu'_{\mathrm{tot}} = (\mu'_{\mathrm{am}} d_{\mathrm{am}} + \mu^{r}_{\mathrm{Ni}} d_{\mathrm{Ni}})/(d_{\mathrm{am}} + d_{\mathrm{Ni}}). \tag{13}$$

From Eqs. (5) we can obtain the susceptibility Ni thickness dependence,

AQ: #4

$$\chi_{\mathrm{tot}} \approx \frac{(\mu^{r\prime}_{\mathrm{am}} d_{\mathrm{am}} + \mu^{r\prime}_{\mathrm{Ni}} d_{\mathrm{Ni}})}{d_{\mathrm{am}} + d_{\mathrm{Ni}}} + \frac{(\alpha_{\mathrm{Ni}} - \alpha_{\mathrm{am}})}{d_{\mathrm{am}} - d_{\mathrm{Ni}}}(\eta_{\mathrm{am}}\lambda_{\mathrm{am}} - \eta_{\mathrm{Ni}}\lambda_{\mathrm{Ni}}) \times \frac{E_{\mathrm{am}} d_{\mathrm{am}} E_{\mathrm{Ni}} d_{\mathrm{Ni}}}{E_{\mathrm{am}} d_{\mathrm{am}} + E_{\mathrm{Ni}} d_{\mathrm{Ni}}}(T - T_e). \tag{14}$$

Figure 6 also illustrates the excellent agreement of the susceptibility dependence on Ni thickness predicted by Eq. (14) with data obtained from the experiment.

Variations of susceptibility and remanence can be ascribed to local anisotropy changes. In a free amorphous FeSiB ribbon, local easy axes are determined by shape and by melt-spun induced frozen-in stresses; on hypothetically free Ni layers, magnetocrystalline anisotropy (along with the distribution of grain orientations) as well as shape set the easy axis directions. Electroplating and subsequent temperature reduction reduces the trilayer longitudinal anisotropy: in the amorphous layer, compressive stress increases everywhere leading to an effective enhancement of transverse anisotropy. In the Ni layers transverse anisotropy appears and increases as a consequence of the increasing applied tensile stress. This mechanism reduces the trilayer response to an external axial field, reducing susceptibility either as temperature drops or Ni thickness increases.

CONCLUSIONS

A bimagnetic ribbon sensing element is here introduced consisting of an inner positive magnetostriction FeSiB amorphous ribbon onto which two symmetrical, negative magnetostriction, Ni layers are grown by electrodeposition. The magnetic behavior has been characterized as a function of temperature and Ni thickness.

The inductance of a coil wounded around the sensing element has been used as the parameter to detect the changes in the magnetic behavior. Within the studied temperature range between 0 and 70 °C, inductance depends linearly on temperature, with sensitivities of the order of 1% K^{-1}. It was found that the sensitivity has a maximum for a Ni thickness of around 25 μm, whose precise value depends on electrodeposition current density.

A simple physical model to interpret the experimentally observed magnetoelastic response of the trilayer has been developed. This model describes semiquantitatively well the dependence of trilayer susceptibility and coil inductance on

Ni thickness d_{Ni} and on temperature. It also predicts and explains the existence of a sensitivity maximum for a finite value of the Ni thickness.

As a microcomposite material for sensors, the proposed bimagnetic trilayer presents the following advantages. (i) The use of MSL (amorphous) and CLs (nickel) with opposite magnetostriction gives rise to a cooperative response leading to an enhanced magnetic sensitivity to temperature changes. According to the model, such enhanced response is given by the factor $(\eta_{am}\lambda_{am}-\eta_{Ni}\lambda_{Ni})$, present in the sensitivity expression. (ii) The enhanced response mentioned in (i) allows one to select trilayer parameters which lead to an optimum inductance response while keeping applied stress at low values, in favorable comparison to materials using nonmagnetic CLs, either making the material more durable for a given working temperature range, or increasing this range for a given durability. (iii) Working under moderate applied stress, as we did, it produces an approximately linear temperature response, which facilitates practical implementation and theoretical analysis. (iv) We expect that electrodeposition of CLs, as compared to gluing them, will produce more robust trilayers and more predictable and repetitive behaviors.

ACKNOWLEDGMENTS

The authors wish to acknowledge partial financial support from CONICET of Argentina and Spanish Ministry of Education and Science (Project No. MAT2004-00150). Also, the authors would like to acknowledge Dr. K. Pirota, J. Torreján, and D. Navas for useful discussions on the fabrication process.

[1]A. Hernando, M. Vázquez, and J. M. Barandiarán, J. Phys. E **21**, 1129 (1988).
[2]A. Inoue, T. Zhang, and A. Takeuchi, Appl. Phys. Lett. **71**, 464 (1997).
[3]M. E. McHenry, M. A. Willard, and D. E. Laughlin, Prog. Mater. Sci. **44**, 291 (1999).
[4]K. Harada, L. Sasada, T. Kawajiri, and M. Inoue, IEEE Trans. Magn. **18**, 1767 (1982).
[5]T. Klinger, H. Pfutzner, P. Schonhuber, K. Hoffmann, and N. Bachl, IEEE Trans. Magn. **28**, 2400 (1992).
[6]L. Mehnen, H. Pfützner, and E. Kaniusas, J. Magn. Magn. Mater. **215**, 779 (2000).
[7]E. Kaniusas, L. Mehnen, C. Krell, and H. Pfützner, J. Magn. Magn. Mater. **215**, 776 (2000).
[8]G. Hinz and H. Voigt, in *Sensors*, edited by W. Gögel, J. Hesse, and J. N. Zemel (VSC, Weinheim, 1989), Vol. 5, Chap. 4, p. 97.
[9]L. Kraus, V. Halar, K. Závta, J. Pokorný, P. Duhaj, and C. Polak, J. Appl. Phys. **78**, 6157 (1995).
[10]E. Kaniusas, L. Mehnen, and H. Pfützner, J. Magn. Magn. Mater. **254**, 624 (2003).
[11]K. Pirota, M. Hernández-Vélez, D. Navas, A. Zhukov, and M. Vázquez, Adv. Funct. Mater. **14**, 266 (2004).
[12]L. Kraus, K. R. Pirota, J. Torrejón, and M. Vázquez, (unpublished). AQ: #5
[13]A. Ibañez and E. Fatás, Surf. Coat. Technol. **191**, 7 (2005).
[14]A. E. Berkowitz, J. L. Walter, and K. F. Wall, Phys. Rev. Lett. **46**, 1484 (1981).
[15]R. Pauthenet, J. Appl. Phys. **53**, 2029 (1982).

AUTHOR QUERIES — 253701JAP

#1 Au: PLEASE USE SPELL OUT FORM OF "C.C."
#2 Au: JAP DOES NOT ALLOW CLAIMS OF NOVELTY. PLEASE CHECK OUR CHANGE.
#3 Au: PLEASE CHECK CHANGES IN Eq. (7)
#4 Au: PLEASE CHECK CHANGES IN Eq. (14)
#5 Au: PLEASE UPDATE REF. 12.